

The design of structural acoustic sensors for active control of sound radiation into enclosures

D S Li^{1,3}, L Cheng² and C M Gosselin¹

¹ Department of Mechanical Engineering, Laval University, Québec, G1K 7P4, Canada

² Research Centre on Noise Abatement and Control, Department of Mechanical Engineering, The Hong Kong Polytechnic University, Hong Kong

E-mail: desheng@mech.ubc.ca

Received 16 September 2002, in final form 29 October 2003

Published 18 February 2004

Online at stacks.iop.org/SMS/13/371 (DOI: 10.1088/0964-1726/13/2/016)

Abstract

This paper introduces a design method for polyvinylidene fluoride (PVDF) structural acoustic sensors for the active control of sound radiation into enclosures. It combines genetic algorithms and the quadratic optimal approach to search for a sensor configuration capable of detecting vibration components with strong sound-radiation ability. In this research, one PVDF sensor is not limited to one single piece of continuous PVDF film. It can consist of a cluster of small PVDF pieces, which could be discrete. Therefore, the parameters to be optimized are the number and the locations of PVDF pieces involved in a sensor. The design method is applied to a cylindrical shell with a floor partition. The general design guidelines are discussed. To show the effectiveness of the method, the control performance of an optimal sensor arrangement is compared with that of non-optimal ones. Physical insights are obtained using structural modal response analysis, modal spectrum analysis of the PVDF sensor output, and structural acoustical coupling analysis. The performance of a PVDF sensor configuration designed at one acoustic resonant frequency is also investigated for other disturbance frequencies below 500 Hz, showing that a significant reduction of acoustic potential energy can be achieved over a wide frequency range. It is demonstrated that, with PVDF sensors optimally designed using the proposed method, the active control of sound radiation into enclosures can be achieved without using acoustic transducers.

1. Introduction

In most active structural acoustic control (ASAC) systems, microphones are usually used as error sensors. In many applications, however, the installation of microphones may not be convenient or may even be very difficult, from the practical point of view. As an alternative, many researchers have been exploring the possibility of using structural error sensors for acoustic control. With the advent of surface-mounted piezoelectric (PZT) actuators and polyvinylidene

fluoride (PVDF) sensors, a more compact and non-intrusive noise control system can be realized if effective design methods are available. As is known, each structural mode contributes differently to the induced sound field. As a result, successful control of the structural vibration may not necessarily lead to an attenuation of the noise. Therefore, structural sensors used for noise control should be properly designed so that they are only (or at least mainly) sensitive to those components with strong sound radiation.

Regarding free-field radiation problems, the relationship between structural vibration and sound radiation is well understood. This knowledge is very helpful for structural sensor design in free-field sound-radiation control. Based on

³ Current address: School of Occupational and Environmental Hygiene and Department of Mechanical Engineering, University of British Columbia, 3rd Floor-2206 East Mall, Vancouver, BC, V6T 1Z3, Canada.

the observation that only one spectral wavenumber component is responsible for the radiation towards a particular given angle [1], Fuller and Burdisso [2] proposed the concept of wavenumber sensing in controlling sound radiation from a simply-supported beam. Later, Maillard and Fuller [3] implemented a sensing configuration using an array of accelerometers to estimate the far-field radiated pressure in a given direction. This was subsequently used in the active control of far-field sound radiation from beams [4], plates [5] and cylinders [6]. Based on the knowledge that only supersonic wavenumber components are responsible for the sound radiation to the far field [7], Wang [8] investigated PVDF-based wavenumber domain sensing techniques for controlling sound radiation from a simply-supported beam. Tanaka *et al* [9] reported another design method for structural acoustic sensors, in which the acoustic power radiated from a plate was first decomposed into a series of acoustic power modes, which contribute independently to the acoustic field. PVDF sensors were then designed according to the shape of the acoustic power modes to be controlled.

As an extension of the work in the free field, Snyder and Tanaka [10] studied the active control of sound transmitted into a coupled rectangular enclosure using the concept of acoustic radiation modes, expressed in terms of a linear combination of natural structural modes. Similar to the acoustic power modes in the free field, acoustic radiation modes are also independent contributors to the sound field, and hence the acoustic potential energy can be reduced by controlling the acoustic radiation modes. Later, Cazzolato and Hansen [11, 12] investigated the practical implementation issues related to sensing acoustic radiation modes. Since this method is based on the acoustic radiation modes, its efficiency can be compromised when structural modal shapes are difficult to express analytically in the case of complex enclosures involved.

As was shown above, the use of structural sensors for controlling sound radiation into the free field has been extensively investigated. As far as the sound radiation into enclosures is concerned, however, there is very limited work reported in the literature. To a great extent, this is due to the complexity resulting from the structural acoustic coupling, which in turn makes the design of structural acoustic sensors more difficult. Hence, further investigation is required.

In this paper, a genetic algorithm (GA)-based method is proposed for designing PVDF structural acoustic sensors to control sound radiation into enclosures. In this method, genetic algorithms (GAs) and the quadratic optimal approach are combined to search for the optimal sensor configuration, which can detect the vibration components with strong sound-radiation ability. Although GAs have been widely used in the location optimization of discrete actuators and acoustic or structural sensors in active noise or vibration control systems in the literature [13–18], to the authors' knowledge, the application of GAs in the design of PVDF structural acoustic sensors for cavity noise control has not been fully explored. It is pertinent to emphasize that the so-called 'one PVDF sensor' in this paper is not limited to one single continuous PVDF piece. It can consist of a cluster of small PVDF pieces, which could be discrete (the discrete pieces can be connected through wires in practical implementations). By varying the number of PVDF pieces, and combining the pieces at different

positions in the sensor, various sensor configurations can be created. The parameters to be optimized are the number and the positions of the set of PVDF pieces involved in the sensor. Therefore, this work is not a simple placement optimization of a single PVDF piece (one sensor in the traditional sense), which is usually not enough for sound-radiation control in enclosures. Genetic algorithms explore a lot of possible configurations to yield the optimal one capable of detecting modes with strong sound-radiation ability. Therefore, it does not require detailed structural acoustic coupling analysis, as do conventional methods used for systems with simple geometry.

The proposed method is applied to a cylindrical shell with a floor partition. Some general design guidelines are first discussed with a single-input and single-output (SISO) control system. Then, to show the effectiveness of the method, the performance with an optimal sensor configuration is compared to those of non-optimal ones. Physical insights are obtained by structural modal response analysis, modal spectrum analysis of the sensor output, and structural acoustic coupling analysis. Finally, to demonstrate the potential of the developed method in dealing with complex problems, a multi-input and multi-output (MIMO) (4 by 4) configuration is designed. The performance of the optimal error sensors designed at one acoustic resonant frequency is also investigated when the structure is under different excitation frequencies below 500 Hz. Numerical results and discussions show that, with PVDF sensors designed using the GA-based method, interior noise control can be achieved without using any acoustic transducers inside the enclosure.

2. Design of PVDF structural acoustic sensors for a cylindrical shell with a floor partition

2.1. Brief introduction to genetic algorithms

As mentioned above, the key issue leading to a successful structural acoustic sensor design is to identify those vibration components that contribute significantly to the acoustic field. Due to their strong search ability in dealing with complex problems, genetic algorithms are used in the proposed approach. The convergence performance of the algorithm was discussed in detail in previous work [19]. For the benefit of readers, a brief introduction to genetic algorithms is given here.

Genetic algorithms are stochastic search techniques based on the mechanism of natural selection and natural genetics [20]. They start with an initial set of random solutions called the initial generation (a set of PVDF sensor configurations, which are coded into binary strings). Each solution in the generation is evaluated by a cost function (the reduction of the acoustic potential energy in the enclosure in this research) and assigned a numerical fitness value (indicating the performance of the PVDF sensor configuration). Then, according to the fitness value, some solutions are selected as parents for reproduction. Those with higher fitness values have a higher probability to be selected, which maintains the rule of 'survival of the fittest'. Through a crossover operator (a process to create children by random copying of information from two parents as shown in figure 2(a)) and/or a mutation operator (a process to create a child by randomly varying the information in a parent as shown in figure 2(b)),

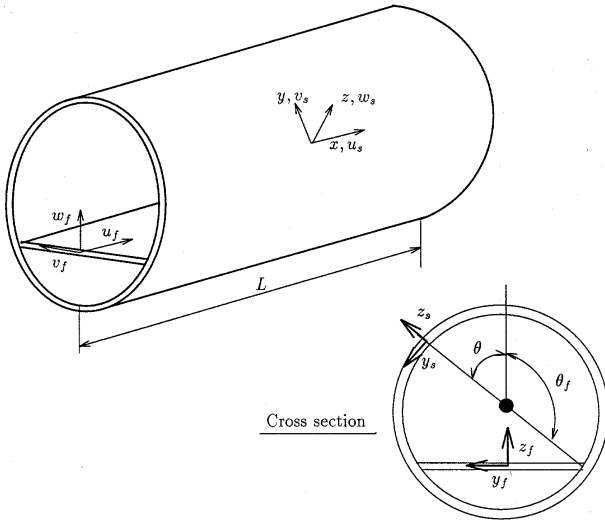


Figure 1. Schematic of a cylindrical shell with a floor partition and the coordinate system.

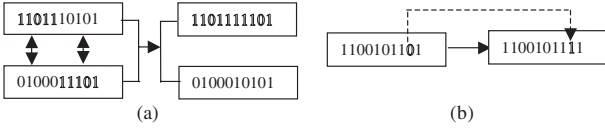


Figure 2. Schematic of the crossover and mutation operators: (a) crossover operator; (b) mutation operator.

offspring (new sensor configurations) are produced to form a new generation. Then, the ‘evolution’ cycle is repeated. After many generations, the search converges to the best individual, which represents the optimal or suboptimal solution to the problem.

In the present investigation, advanced GA techniques, such as the steady state genetic algorithm (SSGA) and the selection method of stochastic remainder sampling (SRS) without replacement [19, 20], are employed to improve the search performance.

2.2. Structural and acoustic models

The structure under investigation is a cylindrical shell with a floor partition, which is shown in figure 1. Both the cylindrical shell and the floor are assumed to have simply-supported boundary conditions at the two ends. The vibroacoustic model of the investigated structure was presented in detail in previous work [21]. In this model, the Rayleigh–Ritz method is used to build the structural model [22] with the coupling between the shell and the floor simulated by an artificial spring system [23]; the sound field induced by the vibration of the structure is simulated using the integro-modal approach [24]; then the structural model and acoustic model are coupled together using acoustoelastic theory [25].

2.3. PVDF sensor output

As an initial condition, a piece of continuous PVDF film is divided into many small rectangular pieces, called elements in this paper. As shown in figure 3(a), it is coded into a binary string, in which each element is represented by one bit with the

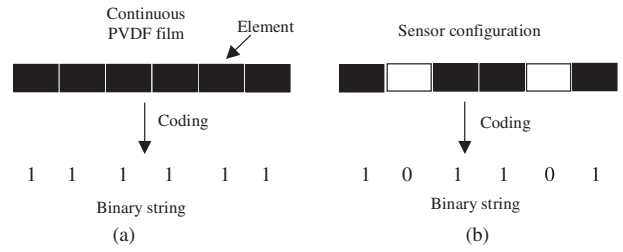


Figure 3. Schematic of the coding of PVDF sensors: (a) a continuous PVDF film; (b) a sensor configuration.

value 1, in the genetic algorithm. A sensor is a combination of some of those elements. In the corresponding binary string, for those removed elements, the corresponding bits are switched to ‘0’. Figure 3(b) shows one sensor configuration and its corresponding string. In figure 3, the small black rectangles denote the remaining elements, and the small white rectangles represent the removed elements in the sensor. Although small gaps seem to exist between adjacent elements, they are only for visualization purposes and do not actually exist. Various sensor configurations can be created via the combinations of different numbers and locations of elements. The voltage output of a sensor can be calculated by

$$V = \sum_{i=1}^n f_i V^i \quad (1)$$

where f_i is the value of the i th bit in the binary string,

$$f_i = \begin{cases} 1 & \text{for the remaining elements} \\ 0 & \text{for the removed elements} \end{cases} \quad (2)$$

V^i is the voltage output of the i th PVDF element, and n is the number of bits in the binary string (i.e., the number of elements in the sensor).

When PVDF is used on the surface of a cylindrical shell structure, under the assumptions of a prominent out-of-plane displacement and negligible temperature effect, the voltage output of a PVDF element in equation (1) can be expressed as [26]

$$V^i = \frac{h_s e_{31}}{\epsilon_{33} A} \int \int_A \left[\frac{w}{R} - \frac{h_s + h_c}{2} \left(\frac{\partial^2 w}{\partial x^2} + \frac{\partial^2 w}{R^2 \partial \theta^2} \right) \right] R \, dx \, d\theta \quad (3)$$

with h_s being the PVDF thickness, e_{31} the piezoelectric material constant, ϵ_{33} the permittivity constant, A the area of a PVDF element, h_c the thickness of the cylindrical shell, R the curvature radius of the cylindrical shell, w the radial displacement of the cylindrical shell, x the longitudinal coordinate and θ the circumferential coordinate.

The out-of-plane displacement function of the cylindrical shell can be expressed as [22]

$$w = v/(j\omega) = \frac{1}{j\omega} \sum_{l=1}^{\infty} v_l \sum_{m=1}^{\infty} \sum_{n=0}^{\infty} \sum_{\alpha=0}^1 C_{mn}^{\alpha} \times \cos\left(n\theta - \frac{\alpha}{2}\pi\right) \sin\left(\frac{m\pi x}{L}\right) \quad (4)$$

where L is the length of the shell, v_l the l th modal magnitude of velocity response, ω the angular frequency, and n and m the

circumferential and longitudinal orders, respectively. $\alpha = 0$ (or 1) means symmetric (or anti-symmetric) mode. C_{mn}^α is the coefficient determined by the free vibration analysis of the investigated structure [22].

Substituting equation (4) into (3), and then substituting the obtained equation into (1), one obtains the voltage output of a sensor as

$$V = \sum_{i=1}^n f_i \frac{h_s e_{31}}{j \varepsilon_{33} A \omega} \sum_{l=1}^{\infty} v_l \sum_{m=1}^{\infty} \sum_{n=0}^{\infty} \sum_{\alpha=0}^1 C_{mn}^\alpha \times \left(1 + \frac{h_s + h_c}{2} \left[\left(\frac{m\pi}{L} \right)^2 R + \frac{n^2}{R} \right] \right) \times \int_A \cos \left(n\theta - \frac{\alpha}{2} \pi \right) \sin \left(\frac{m\pi x}{L} \right) dx d\theta. \quad (5)$$

Let

$$\phi_l = \sum_{i=1}^n f_i \frac{h_s e_{31}}{j \varepsilon_{33} A \omega} \sum_{m=1}^{\infty} \sum_{n=0}^{\infty} \sum_{\alpha=0}^1 C_{mn}^\alpha \times \left(1 + \frac{h_s + h_c}{2} \left[\left(\frac{m\pi}{L} \right)^2 R + \frac{n^2}{R} \right] \right) \times \int_A \cos \left(n\theta - \frac{\alpha}{2} \pi \right) \sin \left(\frac{m\pi x}{L} \right) dx d\theta \quad (6)$$

be the l th modal shape function of the PVDF sensor output, then one can rewrite equation (5) as

$$V = \varphi^T \mathbf{v} \quad (7)$$

where φ is an $(N_m \times 1)$ vector containing the mode shape functions of the PVDF sensor output and \mathbf{v} is an $(N_m \times 1)$ vector containing the modal magnitudes of the velocity response, with N_m being the number of structural modes.

2.4. Determination of the optimal control input using the quadratic optimization approach

For each searched PVDF sensor configuration, the optimal control input of the control system can be determined using the quadratic optimization approach [27]. In this approach, the sum of the squared outputs of the sensors, induced by the primary and control sources, is expressed as a quadratic equation. Then, by minimizing this value, one can obtain the optimal control input. The approach will now be described in detail.

When control is applied, a PVDF sensor measures the combined result induced by the primary and control sources. For the linear system considered here, the voltage output of a PVDF sensor can be expressed as

$$V = V_p + V_c \quad (8)$$

where the subscripts p and c denote the primary and control sources, respectively.

Substituting equation (7) into (8) yields

$$V = \varphi^T \mathbf{v}_p + \varphi^T \mathbf{v}_c \quad (9)$$

where

$$\mathbf{v}_c = \mathbf{Z}_I^{-1} \Psi_{gc} \mathbf{f}_c \quad (10)$$

with \mathbf{Z}_I being a $(N_m \times N_m)$ matrix containing the structural modal impedance, Ψ_{gc} an $(N_m \times N_c)$ matrix of the modal

generalized force transfer functions of the control source, and \mathbf{f}_c an $(N_c \times 1)$ vector containing the control input, with N_c being the number of control sources (PZT actuators in the present case).

Using these expressions, the sum of the squared outputs of the PVDF sensors can be expressed as

$$\sum_{j=1}^{N_e} |V_j|^2 = \mathbf{f}_c^H \mathbf{A} \mathbf{f}_c + \mathbf{f}_c^H \mathbf{b} + \mathbf{b}^H \mathbf{f}_c + c \quad (11)$$

where V_j is the output of the j th PVDF sensor, N_e the number of sensors, and

$$\mathbf{A} = \Psi_{gc}^H \{ \mathbf{Z}_I^{-1} \} \mathbf{Z}_v \mathbf{Z}_I^{-1} \Psi_{gc} \quad (12)$$

$$\mathbf{b} = \Psi_{gc}^H \{ \mathbf{Z}_I^{-1} \} \mathbf{Z}_v \mathbf{v}_p \quad (13)$$

$$c = \mathbf{v}_p^H \mathbf{Z}_v \mathbf{v}_p \quad (14)$$

where \mathbf{Z}_v is the weighting matrix, defined as

$$\mathbf{Z}_v = \varphi_e \varphi_e^T \quad (15)$$

with φ_e being a $(N_m \times N_e)$ matrix whose columns are the vectors of the output modal shape functions of N_e PVDF sensors.

Then, by minimizing the sum of the squared outputs of the PVDF sensors shown in equation (11), one can determine the optimal control input as

$$\mathbf{f}_c = -\mathbf{A}^{-1} \mathbf{b}. \quad (16)$$

With the obtained control input, the residual acoustic potential energy in the enclosure after control is calculated by

$$E = \mathbf{v}^H \mathbf{B}^T \mathbf{Z}_a^H \mathbf{Z}_E \mathbf{Z}_a \mathbf{B} \mathbf{v} \quad (17)$$

where \mathbf{Z}_a is an $(N_n \times N_n)$ diagonal matrix whose elements are calculated by $Z_a(i, i) = \frac{j\rho_0\omega}{\Lambda_i(k_i - k)}$, \mathbf{Z}_E is an $(N_n \times N_n)$ diagonal weighting matrix with elements defined as $Z_E(i, i) = \frac{\Lambda_i}{4\rho_0 c_0}$, \mathbf{B} is an $(N_n \times N_m)$ matrix of modal coupling coefficients between acoustic modes and structural modes, whose elements can be expressed as $B(l, i) = \int_S \psi_l(\mathbf{r}) \phi_i(\mathbf{r}) d\mathbf{r}$, and \mathbf{v} is an $(N_m \times 1)$ vector of structural modal velocities resulting from the primary and control forces. Here, N_n is the number of acoustic modes, and ρ_0 and c_0 the air density and the sound speed in the air, respectively, Λ_i the generalized mass of the i th acoustic mode, k_i and k the wavenumber at the i th acoustic natural frequency and the excitation frequency, respectively, ψ_l the l th structural modal shape function, ϕ_i the i th acoustic modal shape function, S the area of the surrounding structure and \mathbf{r} the position vector.

Subtracting the residual acoustic potential energy from the primary acoustic potential energy, the reduction of acoustic potential energy can be obtained and used as the cost function in the genetic algorithm to evaluate the fitness of this error sensor configuration.

2.5. General design procedure

In the design, the first generation (a set of PVDF sensor configurations) is created randomly. For each PVDF sensor configuration, the fitness value is assigned as described in sections 2.3 and 2.4. The higher the reduction of acoustic potential energy is—while minimizing the sum of the squared outputs of PVDF sensors—the higher will be the fitness value assigned to the sensor configuration. The best PVDF sensor configuration is carried forward to the next generation. Those configurations with higher fitness values (that is, higher acoustic potential energy reduction) have more chance to be selected as parents for reproduction. Hence, generally speaking, the PVDF sensor configurations in the next generation are expected to have better sound-reduction performance than those in the previous generation. At the end of the search, it is expected that an optimal or suboptimal PVDF sensor configuration is found.

3. Numerical results and analysis

Numerical results presented hereafter use the following configuration: the shell and the floor are assumed to have the same thickness of 0.0032 m, a density of 7860 kg m^{-3} , Poisson ratio 0.3, and Young's modulus $2.07 \times 10^{11} \text{ N m}^{-2}$. The cylindrical shell has a length of 1.209 m and a radius of 0.254 m. The sound speed is 343 m s^{-1} , with an air density of 1.2 kg m^{-3} . A modal loss factor of 5×10^{-3} is assigned to both the structure and the cavity. The shell–floor attachment is assumed to be rigid. The position of the floor is defined by $\theta_f = 131^\circ$ (figure 1). The thickness of the PVDF is $5.2 \times 10^{-5} \text{ m}$, with a permittivity constant of $106 \times 10^{-12} \text{ F m}^{-1}$ and a piezoelectric constant of $9.6 \times 10^{-3} \text{ C m}^{-2}$. The genetic algorithm parameters are optimally selected as follows: crossover probability 1.0, mutation rate 0.6, and population size 100 [19].

For computation purposes, the structural displacement and sound pressure decomposition have to be truncated to a finite series. The criteria are the same as those used in the previous work [21]. By a careful convergence study, the number of terms in decomposition series was determined as follows: shell: (8, 10) (longitudinal, circumferential); floor: (8, 5, 5) (transversal, in-plane motion in x , y); cavity: (5, 5, 5) (longitudinal, circumferential, radial).

As is known, the flexural vibration of a circular cylindrical shell involves deformations in both the circumferential and longitudinal (axial) directions. Based on this, strip-type PVDF sensors along the circumferential and the longitudinal directions are used. If the whole structural surface were covered with PVDF film, it would be very computationally intensive, because of the large number of bits required to represent the large number of elements in binary strings.

In the following sections, the general design guidelines are first investigated using a SISO control system. The effectiveness of the GA-based method is then demonstrated by comparing the performance of an optimal sensor with those of non-optimal ones. Physical insights are obtained using structural modal response analysis, modal spectrum analysis of the sensor output, and structural acoustic coupling analysis. Finally, to show the potential of the design method in dealing

with MIMO control systems, the error sensors in a MIMO (4 by 4) ASAC system are designed for the investigated structure. In all cases, PZT actuators, which are assumed to operate in an in-plane force model due to its high performance in controlling the interior noise of a cylindrical shell structure [19], provide both the primary and control vibration sources. The size of the PZT actuators is 0.05 m long in the longitudinal direction by 0.018 m (i.e., with sector angle coverage of 4°) wide in the circumferential direction. The location of the control actuators has been optimized using the method presented in previous work [19] and is used directly here. The positions of actuators and sensors are denoted by two indices (x, θ) , where x and θ are the coordinates in the longitudinal and the circumferential directions on the structural surface, respectively. The size of PVDF elements is represented by $(\Delta x, \Delta \theta)$, where Δx is the length covered in the longitudinal direction and $\Delta \theta$ the sector angle coverage in the circumferential direction.

3.1. Investigation of general design guidelines

As mentioned before, a continuous PVDF film is divided into small elements during the design. Smaller elements need more bits in the strings and, therefore, increase the demand for computation. For the given structure, this issue is first discussed using a SISO system. The structure is assumed to be excited by two actuators located at $(0.30 \text{ m}, 90^\circ)$ and $(0.5 \text{ m}, 120^\circ)$. The control actuator is located at $(0.58 \text{ m}, 296^\circ)$. The sensor is designed at an acoustic resonant frequency of 283.7 Hz.

3.1.1. The effect of the circumferential dimension of elements in circumferential strip-type sensors. First, we study the effect of the element dimension in the circumferential direction on the sensor performance. As the initial configuration, a piece of continuous strip-type PVDF film, with longitudinal dimension 0.1 m and sector angle coverage 360° , is attached to the cylindrical shell surface along the circumferential direction (figure 4(a)). In figure 4, the shell surface is cut along the longitudinal direction at $\theta = 0^\circ$ and stretched into a planar surface. Small rectangles represent the disturbance actuators, a small ellipse denotes the control actuator (actually the control actuator is a rectangular plate with the same size as the disturbance actuators), and large black rectangles represent PVDF elements. The longitudinal position of this PVDF sensor on the structural surface is $x = 0.8 \text{ m}$. It should be noted that the investigation has shown that the longitudinal location of a circumferential strip-type PVDF sensor does not significantly affect the control performance. Therefore, the choice of location x is flexible, provided that it does not overlap with the PZT actuators and is not too close to the ends of the structure. Three different element sizes—i.e., $(0.1 \text{ m}, 45^\circ)$, $(0.1 \text{ m}, 30^\circ)$, and $(0.1 \text{ m}, 20^\circ)$ —are investigated.

The optimal sensor configuration obtained with the element size $(0.1 \text{ m}, 45^\circ)$ is shown in figure 4(b). It is composed of three PVDF elements. Although the three elements are separate, they are considered as one sensor with output calculated by equation (1). In a practical implementation, they are connected together by wires. Two other optimal configurations using smaller elements of $(0.1 \text{ m}, 30^\circ)$ and $(0.1 \text{ m}, 20^\circ)$ are given in figures 4(c) and (d), respectively.

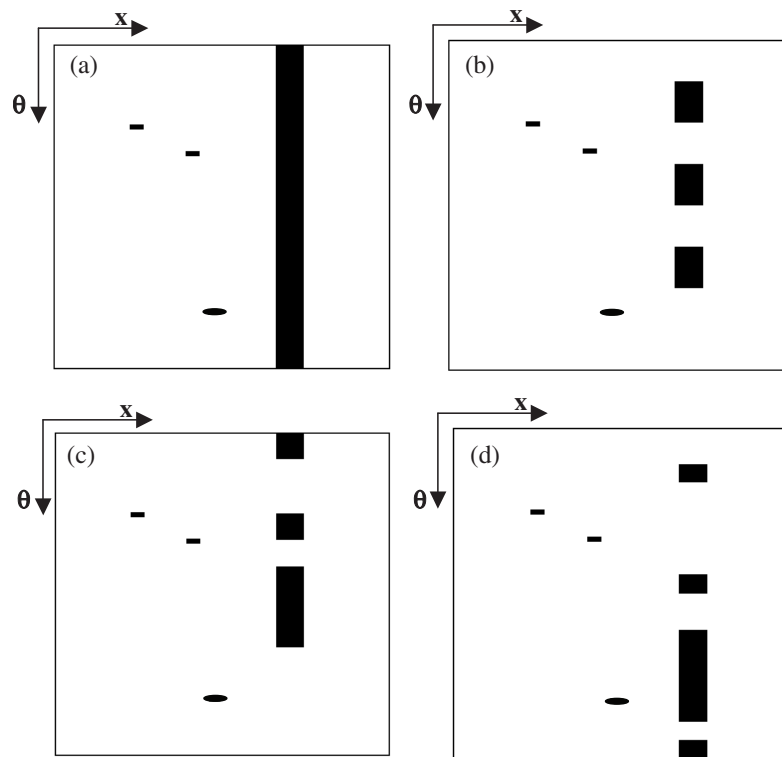


Figure 4. Optimal configurations of a PVDF sensor designed with different circumferential element sizes: (a) initial configuration of the sensor before design; (b) element size (0.1 m, 45°); (c) element size (0.1 m, 30°); (d) element size (0.1 m, 20°); ■, disturbance; ●, control; ■, sensor.

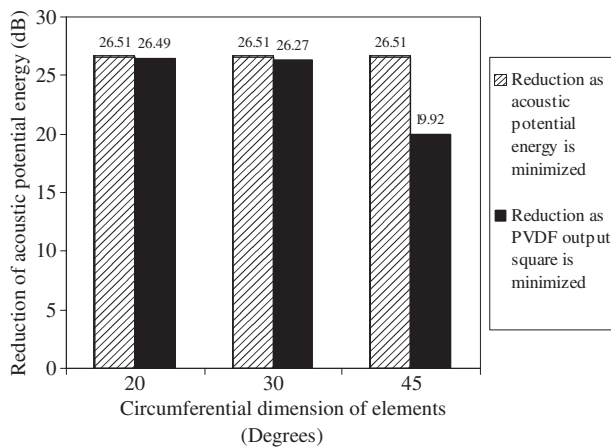


Figure 5. The effect of the circumferential dimension of elements on the performance of a designed PVDF sensor.

The primary acoustic potential energy in the enclosure is 76.78 dB. The control performances based on the three error sensors are compared in figure 5. It can be seen that a 19.92 dB reduction can be achieved with the (0.1 m, 45°) element case. Reductions with the two other configurations are, respectively, 26.27 and 26.49 dB, which are much higher than the previous case. Therefore, one can argue that as elements with smaller circumferential dimensions are used in the sensor design, better performance can be expected.

This difference in sound reduction is due to the difference in the sensor configurations, which leads to different abilities

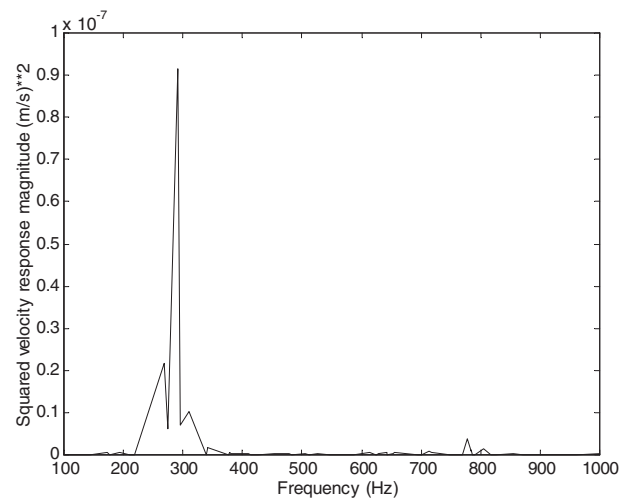


Figure 6. Structural modal response spectrum at the design frequency.

in detecting structural modes with strong sound radiation. In order to show this, the modal spectrum of the structural response is shown in figure 6. Since no structural and acoustic modes exist below 100 Hz, the frequency axis starts at 100 Hz. From this figure, one can see that three structural modes at 267.8, 290.5, and 310.5 Hz have significant contribution to the structural vibration, and that the 290.5 Hz mode is the dominant one. The structural acoustic coupling analysis shows that the coupling coefficients between the three structural modes at 267.8, 290.5, and 310.5 Hz and the acoustic mode at 283.7 Hz

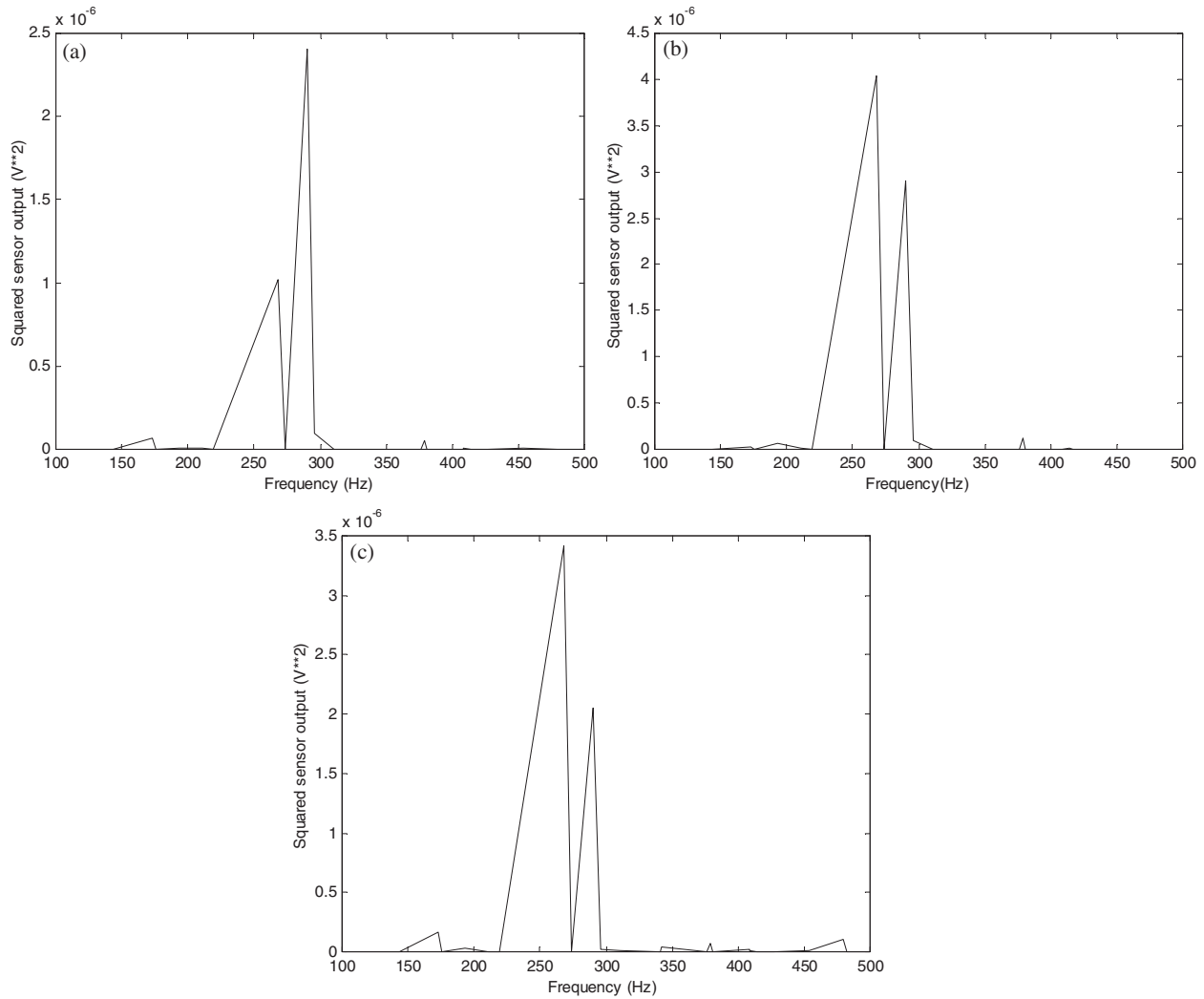


Figure 7. Modal spectra of the three sensor outputs: (a) element size (0.1 m, 45°); (b) element size (0.1 m, 30°); (c) element size (0.1 m, 20°).

are 0.060 338, 0.000 492, and 0.023 806, respectively. The coupling coefficient is a measure of the spatial match between a structural mode and an acoustic mode, and is defined as the integral of the product between a structural mode and an acoustic mode over the whole vibrating surface [28]. Clearly, the 267.8 Hz mode has much higher sound-radiation ability than the two other modes. Therefore, although the 290.5 Hz mode dominates the structural vibration, the 267.8 Hz mode is the one that should be sensed and controlled to achieve significant sound reduction. Figure 7 shows the output of the three sensor configurations. It can be seen that the 290.5 Hz mode dominates the sensor output with (0.1 m, 45°) (figure 7(a)), whilst for the other two sensor configurations with smaller elements, the 267.8 Hz mode is prominent in the output of the sensors (figures 7(b) and (c)). This shows that optimal sensors designed using smaller circumferential element size have stronger ability to selectively sense the structural modes with high sound radiation. This explains why optimal sensors with smaller elements tend to give higher sound reduction.

Besides the absolute value of sound reduction, an alternative for evaluating a sensor is to compare the sound reduction with the theoretical upper limit for a given control

actuator configuration. This upper limit can be obtained by minimizing the acoustic potential energy [19]. In practice, the sensor, which can measure the acoustic potential energy in the enclosure, does not exist. However, if a PVDF sensor is properly designed, it should be possible to approach this limit. For the control actuator configuration shown in figure 4, the theoretical upper limit of sound reduction is 26.51 dB. One can observe from figure 5 that the sound reductions based on the strip-type sensors with element size (0.1 m, 30°) and (0.1 m, 20°) are already very close to the theoretical upper limit. Therefore, it is not necessary to cover the whole structural surface with PVDF film. Considering the computational cost associated with the number of elements, the circumferential element size is chosen to be 30° in the following investigation.

3.1.2. The effect of the longitudinal dimension of a circumferential strip-type PVDF sensor. To investigate the influence of the longitudinal dimension of strip-type PVDF sensors attached along the circumferential direction of the cylindrical shell, two longitudinal dimensions—i.e., 0.02 and 0.2 m—are tested here. Likewise, the sensor is divided into elements in the circumferential direction, each of which

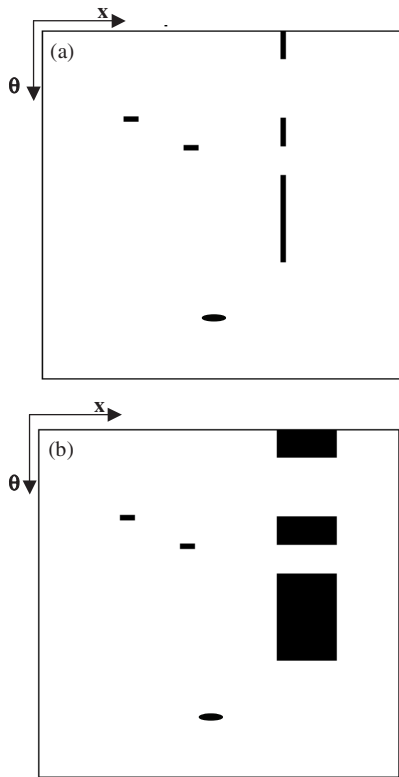


Figure 8. Optimal configurations of a PVDF sensor designed with different longitudinal element sizes: (a) element size (0.02 m, 30°); (b) element size (0.2 m, 30°); ■, disturbance; ●, control; ▨ and ■, sensor.

covers a sector angle of 30°. The optimal error sensor configurations obtained are shown in figures 8(a) and (b), respectively. The configuration with a longitudinal dimension of 0.1 m previously used in figure 4(c) is also used for comparison purposes. Comparing all three configurations shown in figures 4(c), 8(a) and (b), one can see that their circumferential configurations are identical. Hence, a larger longitudinal dimension means a larger PVDF coverage of a sensor. Figure 9 demonstrates the reductions of the acoustic potential energy achieved based on the error signals from the three optimal sensors. They are 24.63, 26.27, and 26.2 dB, while the longitudinal dimensions of the sensors are 0.02, 0.1, and 0.2 m, respectively. Using the smallest sensor of the three, the sound reduction is 24.63 dB, which is 1.88 dB less than the upper limit of reduction. With a larger longitudinal dimension of 0.1 m, the sound reduction (i.e., 26.27 dB) is improved slightly and closely approaches the upper limit of sound reduction (i.e., 26.51 dB). As one continues to increase the longitudinal dimension to 0.2 m, no further improvement is observed. Therefore, the results seem to indicate that the PVDF coverage along the longitudinal direction does not have a significant influence on the control performance.

According to this observation, one would suspect that the performance of a longitudinal strip-type PVDF sensor might not be as good as that of a circumferential one. To investigate this, a continuous strip-type PVDF film with a sector angle coverage of 30°, which is located at $\theta = 50^\circ$ from $x = 0.05$ to 1.15 m along the longitudinal direction, is used as the initial configuration. During the sensor design, the whole strip along

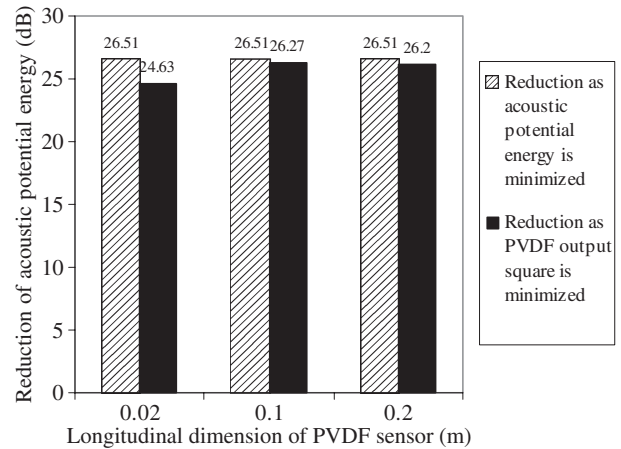


Figure 9. The effect of the longitudinal dimension of a strip-type PVDF sensor along the circumferential direction.

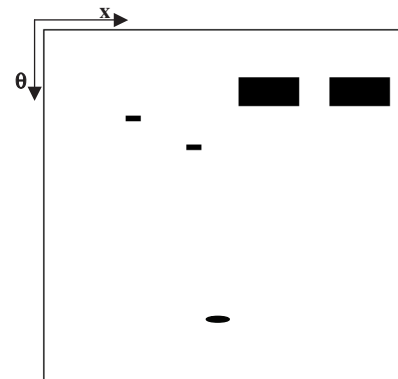


Figure 10. Optimal configuration of a longitudinal strip-type PVDF sensor; ■, disturbance; ●, control; ■, sensor.

the longitudinal direction is divided into elements of (0.1 m, 30°). Figure 10 shows the optimal sensor configuration. By minimizing the squared output of this sensor, the reduction of acoustic potential energy achieved is only 12.10 dB, which is much lower than that (i.e., 26.27 dB) obtained using a circumferential PVDF strip.

The investigation demonstrates that the circumferential modal response of the structure plays a key role in the sound radiation into enclosures in the low-frequency range. This is consistent with the observation in the previous investigation using a plain cylindrical shell, indicating that circumferential modes are more strongly coupled to the cavity than longitudinal ones, in the low-frequency range. Therefore, if only one sensor is used for the noise control of cylindrical shell structures, it should be attached to the structural surface along the circumferential direction. Other simulations were also performed using different circumferential positions of the longitudinal strip-type sensors. The results show consistent observations.

3.2. Performance comparison between the optimal and non-optimal sensor configurations

To show the effectiveness of the GA-based method, the performance of the optimal error sensor shown in figure 4(c) is compared to three random configurations. The disturbance

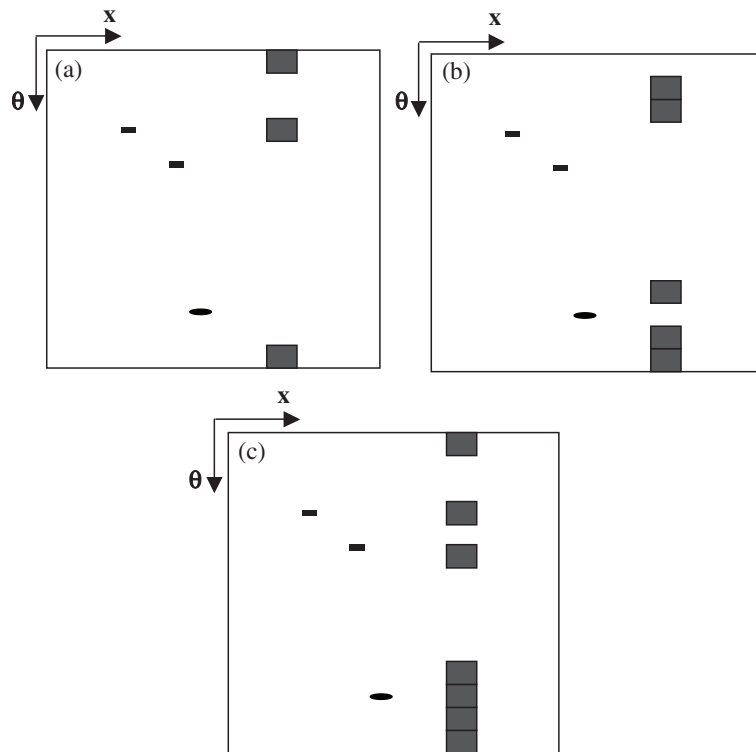


Figure 11. Configurations of non-optimal sensors: (a) non-optimal sensor 1 consisting of three PVDF elements; (b) non-optimal sensor 2 consisting of five PVDF elements; (c) non-optimal sensor 3 consisting of seven PVDF elements; ■, disturbance; ●, control; ■, sensor.

and control actuator arrangements are the same for the four cases. The optimal sensor consists of five elements as shown in figure 4(c). Three non-optimal sensors are composed of three, five and seven elements as demonstrated in figures 11(a), (b) and (c) respectively. In all configurations, the size of a PVDF element is 0.1 m along the longitudinal direction and 0.133 m (i.e., sector angle 30°) along the circumferential direction. Figure 12 shows the reductions in acoustic potential energy in the cavity obtained by minimizing the squared output of the PVDF sensors at the design frequency. It can be seen that the optimal sensor configuration gives a reduction of 26.27 dB, whilst its counterparts yield 6.91, 13.43 and 11.38 dB respectively. Obviously, the optimal sensor outperforms the three non-optimal sensors, irrespective of the actual size of the sensors.

The modal spectra analysis of the sensor outputs further confirms the superiority of the optimal sensor in capturing structural modes with strong sound-radiation ability (figure 13). From figure 13(a), one can notice that the optimal sensor detects effectively the structural mode at 267.8 Hz, which has the strongest sound-radiation ability, as shown in section 3.1.1. The non-optimal sensors either have a very weak response to this structural mode (figures 13(b) and (c)) or cannot detect this mode (figure 13(d)) at all. This explains why much higher sound reduction can be achieved with the optimal sensor.

3.3. The design of PVDF sensors in multi-input and multi-output (MIMO) ASAC systems

When a structure is under complex disturbance, a MIMO control system is needed to achieve satisfactory sound

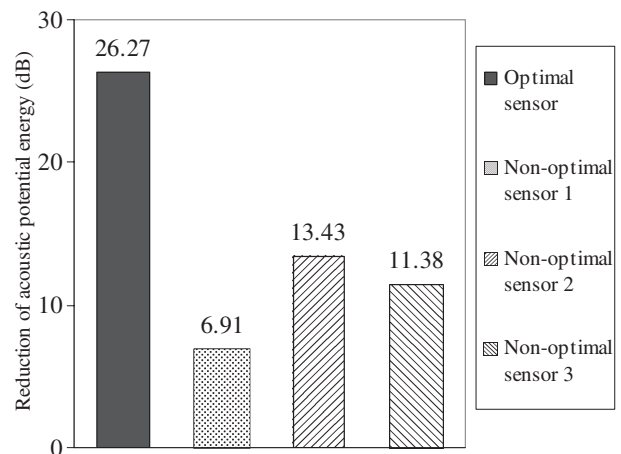


Figure 12. Performance comparison between optimal and non-optimal sensors.

attenuation. To show the potential of the GA-based method in dealing with such cases, PVDF error sensors in a 4 × 4 control system are designed as the structure is excited by 10 PZT actuators randomly located on the structural surface at an acoustic resonant frequency of 283.7 Hz. Four control actuators are located at (0.19, 97°), (0.77, 95°), (0.72, 61°), and (0.72, 120°). As the initial configuration, four strip-type PVDF films are attached to the surface of the shell. Two of them are along the circumferential direction, located at $x = 0.8$ and 0.95 m, respectively, with size 0.1 m wide in the longitudinal direction and 1.60 m (i.e., sector angle 360°) long along the circumferential direction. The two others

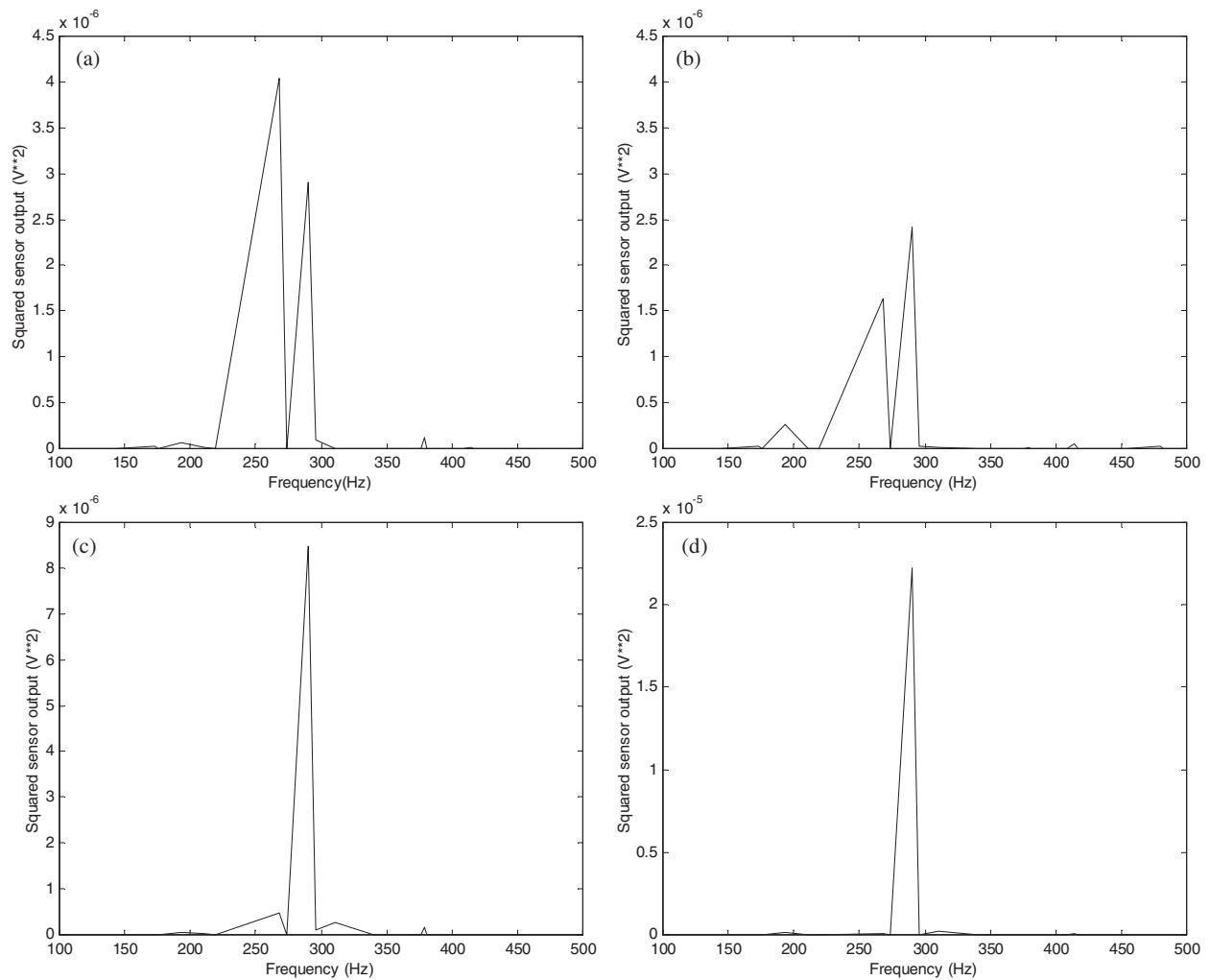


Figure 13. Modal spectra of the optimal and non-optimal sensor output: (a) optimal sensor; (b) non-optimal sensor 1; (c) non-optimal sensor 2; (d) non-optimal sensor 3.

are along the longitudinal direction, located at $\theta = 10^\circ$ and 300° , respectively, with size 1.10 m long and 0.133 m wide (i.e., sector angle 30°). This initial configuration is shown in figure 14(a). It should be noted that the initial locations of the sensors are selected from the possible positions on the structural surface, without overlapping with PZT actuators, because the longitudinal position of a circumferential sensor and the circumferential position of a longitudinal sensor have little influence on control performance.

In the design process, the element size of (0.1 m, 30°) is used. After the optimization design, the optimal configuration of sensors is given in figure 14(b). The remaining PVDF elements along one strip, whether they are continuous or discrete, still belong to one sensor, amounting to four error sensors in total. Using this configuration, a reduction of 54.58 dB is achieved in acoustic potential energy, which is only 0.92 dB less than the upper limit of 55.50 dB. Again, with the optimal strip-type PVDF sensors, very good control performance is achieved.

Up to this point, the performance of the optimal sensor configuration has been tested at the design frequency. However, if the sensor arrangement is only effective at one particular frequency, the applicability of the control system

may be greatly compromised. Therefore, simulations were carried out to see whether the sensor configuration shown in figure 14(b) could also be effective at other disturbance frequencies. Since there are no structural or acoustic modes below 100 Hz, the control performance is only shown over the frequency range between 100 and 500 Hz in figure 15. In this figure, the solid curve represents the acoustic potential energy of the primary field, the dotted curve denotes the residual acoustic potential energy obtained by minimizing the sum of the squared output of the optimal PVDF error sensors, and the dashed curve represents the residual acoustic potential energy obtained by minimizing the acoustic potential energy in the enclosure. It can be seen that, in the vicinity of the design frequency, which is 283.7 Hz in the present case, the sound reduction achieved based on the error signal from the optimal PVDF sensors is very close to the upper limit achieved by minimizing the acoustic potential energy. As the disturbance frequency deviates from the design frequency, significant reduction can still be obtained to some extent in most cases in the low-frequency range. Structural acoustic coupling analysis demonstrates that the low-frequency sound field is induced mainly by a limited number of structural modes [28]. Therefore, it is possible to achieve sound

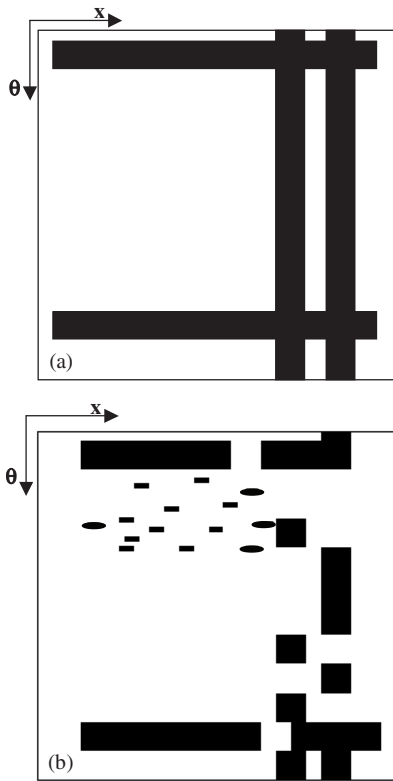


Figure 14. Optimal configuration of the PVDF error sensors in a 4×4 control system: (a) initial configuration of the PVDF error sensors before design; (b) optimal configuration of the PVDF error sensors after design; ■, disturbance; ●, control; ■, sensor.

attenuation over a wide frequency range with an optimal sensor configuration designed at one particular frequency. Two exceptions occur at 142 and 379 Hz, where no attenuations are achieved. Analysis shows that 141.9 Hz is an acoustic resonance with longitudinal order 1. Figure 16 shows the modal spectrum of the sensor output. It can be observed that the structural mode at 172.9 Hz is prominent in the output signal. Further analysis demonstrates that its longitudinal order is also 1. According to the structural acoustic coupling characteristics of the investigated structure [28], the structure-acoustic coupling between an acoustic mode and a structural mode can happen only if their longitudinal orders are an odd and even combination. In the present case, there is no coupling between the structural mode captured by the sensor and the acoustic mode to be controlled, which explains the ineffectiveness of the sensor at this particular frequency. A similar phenomenon occurs at 379 Hz. The sensor detects mainly the 378.7 Hz structure mode, as evidenced by figure 17. However, the structural mode at 378.7 Hz (longitudinal order 2) and the acoustic mode at 378.9 Hz (longitudinal order 0) are not coupled to each other. Nevertheless, the investigation shows that, for the investigated structure, the frequency dependence of a sensor configuration is not very strong, showing the possibility of optimizing a sensor configuration for a broadband disturbance.

As a final note, two points are worth mentioning. First, investigations using different disturbances, control actuator configurations and design frequencies lead to the same conclusions. Second, by optimally tuning the parameters

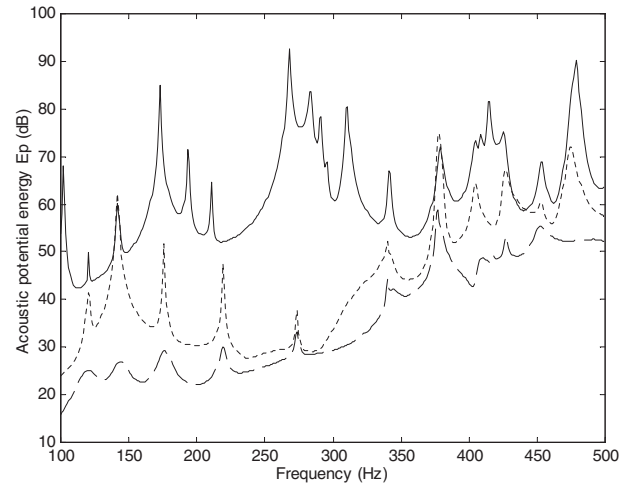


Figure 15. Control performance of the optimal PVDF sensors in the low-frequency range. —, primary acoustic potential energy in the enclosure; ·····, residual acoustic potential energy while the sum of the squared output of the optimal PVDF sensors is minimized; ---, acoustic potential energy minimized.

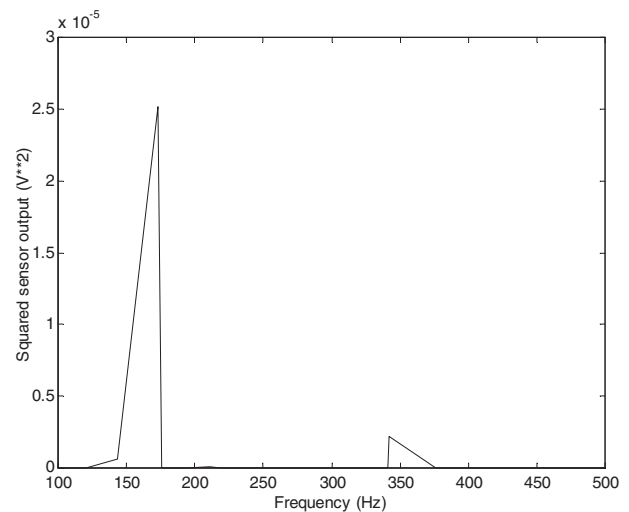


Figure 16. Modal spectrum of the optimal sensor output with the disturbance at 142 Hz.

involved in the genetic algorithm, one can significantly improve the convergence performance [19]. However, because of the statistic nature of genetic algorithms, systematic convergence to the global optimum is not guaranteed in each search. In this research, the optimization operation was run for ten times in each case to make sure that a global optimum can be found. For SISO control systems, every run reached the global optimum. In the case of MIMO control systems, the global optimum was reached in most runs.

4. Conclusions

In this paper, a genetic algorithm (GA)-based method is proposed for designing PVDF structural acoustic sensors to control sound radiation into enclosures. Genetic algorithms are introduced to search for the optimal PVDF sensor configuration, which can detect the vibration components with high sound-radiation ability. The cost function is the reduction

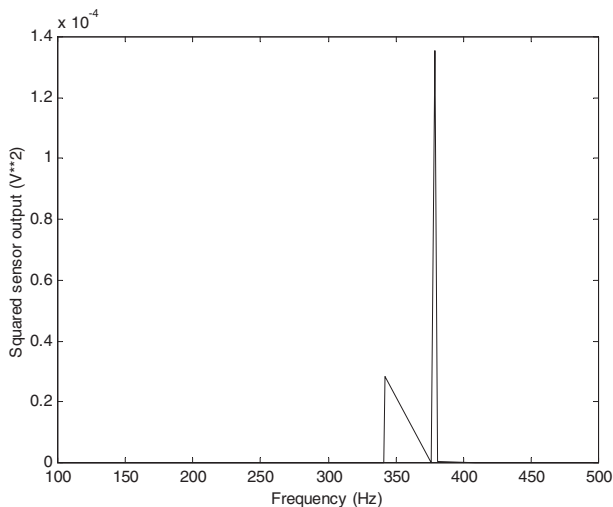


Figure 17. Modal spectrum of the optimal sensor output with the disturbance at 379 Hz.

of acoustic potential energy inside the cavity achieved by minimizing the sum of the squared outputs of PVDF error sensors. When structural and acoustic modal shapes are difficult to express analytically, this method is believed to be more suitable for PVDF sensor design than existing analytical methods, which require the knowledge of the structural mode shapes for the design.

The method and its performance were demonstrated using a cylindrical shell with a floor partition, leading to the following conclusions.

- (1) The circumferential arrangement of PVDF elements can significantly influence the control performance. A smaller circumferential element dimension tends to produce a sensor with stronger ability to sense the vibration components efficiently radiating sound into the cavity.
- (2) As in the case of a pure cylindrical shell, the circumferential modal response of a cylindrical shell with a floor also plays a key role in radiating sound into the enclosure in the low-frequency range. Higher sound attenuation can be achieved using a circumferential strip-type sensor rather than a longitudinal one.
- (3) Based on the error signal from optimal sensors, the reduction of acoustic potential energy can be very close to the upper limit predicted by minimizing the acoustic potential energy in the cavity. Since the latter is used only as the evaluation criterion in the design, active control of sound radiation in enclosures can be realized without using any acoustic sensors.
- (4) For the investigated structure, the PVDF structural acoustic sensors designed at one acoustic natural frequency also perform well for other disturbance frequencies in the low-frequency range.

The investigation has shown the strong ability of the GA-based method in designing PVDF sensors for sound-radiation control in enclosures when the structure is subject to a narrowband disturbance. It would be of great interest to extend the design method to broadband disturbances in future work.

Acknowledgments

The work described in this paper was supported by NSERC Canada and the Research Grants Council of the Hong Kong Special Administrative Region (Grant: PolyU 5165/02E).

References

- [1] Junger M C and Feit D 1986 *Sound, Structures and their Interaction* (Boston, MA: MIT Press)
- [2] Fuller C R and Burdisso R A 1991 A wavenumber domain approach to the active control of structure-borne sound *J. Sound Vib.* **148** 355–60
- [3] Maillard J P and Fuller C R 1994 Advanced time domain wave-number sensing for structural acoustic systems. I. Theory and design *J. Acoust. Soc. Am.* **95** 3252–61
- [4] Maillard J P and Fuller C R 1994 Advanced time domain wave-number sensing for structural acoustic systems. II. Active radiation control of a simply supported beam *J. Acoust. Soc. Am.* **95** 3262–72
- [5] Maillard J P and Fuller C R 1995 Advanced time domain wave-number sensing for structural acoustic systems. III. Experiments on active broadband radiation control of a simply-supported plate *J. Acoust. Soc. Am.* **98** 2613–21
- [6] Maillard J P and Fuller C R 1999 Active control of sound radiation from cylinders with piezoelectric actuators and structural acoustic sensing *J. Sound Vib.* **222** 363–88
- [7] Maidanik G 1974 Vibrational and radiative classification of modes of a baffled finite panel *J. Sound Vib.* **34** 447–55
- [8] Wang B T 1998 The PVDF-based wave number domain sensing techniques for active sound radiation control from a simply supported beam *J. Acoust. Soc. Am.* **103** 1904–15
- [9] Tanaka N, Kikushima Y, Kuroda M and Snyder S D 1976 Active control of acoustic power radiated from a vibrating planar structure using smart sensors. (Acoustic power suppression using adaptive feedforward control.) *JSME Int. J. C* **39** 49–57
- [10] Snyder S and Tanaka N 1993 On feedforward active control of sound and vibration using error signals *J. Acoust. Soc. Am.* **94** 2181–93
- [11] Cazzolato B S and Hansen C H 1998 Active control of sound transmission using structural error sensing *J. Acoust. Soc. Am.* **104** 2878–89
- [12] Cazzolato B S and Hansen C H 1998 Structural radiation mode sensing for active control of sound radiation into enclosed spaces *J. Acoust. Soc. Am.* **106** 3732–5
- [13] Katsikas S K, Tsalhalis D, Manolas D and Xanthakis S 1995 A genetic algorithm for active noise control actuator positioning *Mech. Syst. Signal Process.* **9** 697–705
- [14] Baek K H and Elliott S J 1995 Natural algorithms for choosing source location in active control systems *J. Sound Vib.* **186** 245–67
- [15] Martin T and Roure A 1998 Active noise control of acoustic sources using spherical harmonics expansion and a genetic algorithm: simulation and experiment *J. Sound Vib.* **212** 511–23
- [16] DeFonseca P, Sas P and Brussel H 1997 Optimisation methods for choosing sensor and actuator locations in an actively controlled double-panel partition *Proc. SPIE* **3041** 124–35
- [17] Lecce L, Ovallesco A, Concilio A and Sorrentino A 1995 Optimal positioning of sensors using genetic algorithms in an active noise control system with piezoelectric actuators *Proc. Topical Symp. VI on Intelligent Materials and Systems of the 8th CIMTEC World Ceramics Conf. and Forum on New Materials (Florence)* pp 307–14
- [18] Manolas D A, Gialamas T and Tsalhalis D T 1996 A genetic algorithm for the simultaneous optimization of the sensor and actuator positions for an active noise and/or vibration control system *Proc. Inter Noise 96 (Liverpool)* pp 1187–91

- [19] Li D S, Cheng L and Gosselin C 2004 Optimal design of PZT actuators in active structural acoustic control of a cylindrical shell with a floor partition *J. Sound Vib.* **269** 569–88
- [20] Goldberg D E 1998 *Genetic Algorithms in Search, Optimization and Machine Learning* (Reading, MA: Addison-Wesley)
- [21] Missaoui J and Cheng L 1998 Vibroacoustic analysis of a finite cylindrical shell with internal floor partition *J. Sound Vib.* **215** 1165–79
- [22] Missaoui J, Cheng L and Richard M J 1996 Free and forced vibration of a cylindrical shell with a floor partition *J. Sound Vib.* **190** 21–40
- [23] Cheng L 1996 Vibroacoustic modeling of mechanically coupled structures: artificial spring technique applied to light and heavy medium *Shock Vib.* **3** 193–200
- [24] Missaoui J and Cheng L 1997 A combined integro-modal approach for prediction of acoustic properties of irregular-shaped cavities *J. Acoust. Soc. Am.* **101** 3313–21
- [25] Dowell E H, Gonnar G F III and Smith D A 1977 Acoustoelasticity: general theory, acoustic natural modes and forced response to sinusoidal excitation, including comparisons with experiment *J. Sound Vib.* **52** 519–42
- [26] Tzou H S, Bao Y and Venkayya V B 1996 Parametric study of segmented transducers laminated on cylindrical shells. Part I. Sensor patches *J. Sound Vib.* **197** 207–24
- [27] Hansen C H and Snyder S D 1997 *Active Control of Noise and Vibration* (E&Fn Spon)
- [28] Li D S, Cheng L and Gosselin C 2002 Analysis of structural acoustic coupling of a cylindrical shell with an internal floor partition *J. Sound Vib.* **250** 903–921